J. Fluid Mech. (2002), *vol.* 470, *pp.* 135–149.
DOI: 10.1017/S002211200200191X Printed in the United Kingdom

Determination of surface shear viscosity via deep-channel flow with inertia

By A. H. HIRSA[1], J. M. LOPEZ[2] AND R. MIRAGHAIE[1]

[1]Department of Mechanical, Aerospace and Nuclear Engineering, Rensselaer Polytechnic Institute, Troy, NY 12180, USA

[2]Department of Mathematics and Statistics, Arizona State University, Tempe, AZ 85287, USA

(Received 23 April 2001 and in revised form 1 May 2002)

Results of an experimental and computational study of the flow in an annular region bounded by stationary inner and outer cylinders and driven by the rotation of the floor are presented. The top is a flat air/water interface, covered by an insoluble monolayer. We develop a technique to determine the surface shear viscosity from azimuthal velocity measurements at the interface which extends the range of surface shear viscosity that can be measured using a deep-channel viscometer in the usual Stokes flow regime by exploiting flow inertia. A Navier–Stokes-based model of bulk flow coupled to a Newtonian interface that has surface shear viscosity as the only interfacial property is developed. This is achieved by restricting the flow to regimes where the surface radial velocity vanishes. The use of inertia results in an improved signal-to-noise ratio of the azimuthal velocity measurements by an order of magnitude beyond that available in the Stokes flow limit. Measurements on vitamin K_1 and stearic acid monolayers were performed, and their surface shear viscosities over a range of concentrations are determined and found to be in agreement with data in the literature.

1. Introduction

Surfactant hydrodynamics plays an important role in various fields, ranging from biomedical applications such as lung surfactant therapy (Grotberg 1994) to numerous industrial applications (Edwards, Brenner & Wasan 1991). We are interested in investigating the intrinsic interfacial properties of surfactant-influenced gas/liquid interfaces, in particular the air/water interface.

The coupling between the liquid subphase and the interface in the presence of a monomolecular surfactant film (monolayer) has been the subject of numerous studies (e.g. see Slattery 1990; Edwards *et al.* 1991). The description of the interfacial flow generally requires a constitutive relation for the interfacial stress (for the bulk flow we already have the Navier–Stokes equations), and this constitutive relation leads to the concept of intrinsic surface viscosities (Boussinesq 1913; Scriven 1960; Aris 1962).

Various methods have been developed for the measurement, in particular, of the surface shear viscosity, μ^s, the two-dimensional counterpart of (shear) viscosity in the bulk fluid, μ. Many of these methods are described in Edwards *et al.* (1991, chap. 7). These include the single knife-edge method and its derivatives, where the interface is sheared and the torque on the circular knife-edge is measured. Although these methods are experimentally robust, the analysis of the results generally lacks

the coupling with the bulk flow. The sensitivity of these types of surface viscometers is limited to about 10^{-2} surface Poise, sP ($\mathrm{g\,s^{-1}}$).

Many surface chemists have used planar flows to quantify the 'interfacial viscosity', such as the surface-pressure driven flow in a slit channel (Gaines 1966). A drawback of methods that use planar geometries is that the surface shear and dilatational viscosities appear as a sum. Thus, the determination of surface shear viscosity depends on knowledge of the surface dilatational viscosity, κ^s, consistent measurements of which have yet to appear in the literature. Sacchetti, Yu & Zografi (1993) have made direct velocity measurements in the plane of the interface in a slit channel, validating the predictions made by an early theory on the hydrodynamic coupling of the interface by Harkins & Kirkwood (1938). Surface viscosity data deduced from the measurements are reported to be sensitive down to order 10^{-4} sP. Schwartz, Knobler & Bruinsma (1994) have also measured the interfacial velocity for a monolayer film driven in a channel. The determination of surface viscosity, $(\mu^s + \kappa^s)$, from the slit channel flow is possible for a limited range of bulk to surface viscosity ratios. Stone (1995) has considered this problem theoretically for a large range of surface viscosity to bulk (shear) viscosity ratios.

Stone & Ajdari (1998) provide an exact solution for the related problem of a solid disk embedded in a monolayer-covered gas/liquid interface coupled to a subphase of finite viscosity. They provide results for the full range of surface viscosity to bulk viscosity ratios. Barentin, Ybert & Di Meglio (1999) use this theory to measure the surface shear viscosities of adsorbed and deposited monolayers.

The shortcoming due to the surface viscosity appearing as the sum $(\mu^s + \kappa^s)$ in planar flows was overcome by the method developed by Mannheimer & Schechter (1970), known as the deep-channel surface viscometer. The deep-channel is an annular flow region bounded by stationary inner and outer cylinders and is driven by the constant (slow) rotation of the floor at $\Omega\,\mathrm{rad\,s^{-1}}$, while the surface is covered by a monolayer (adsorbed or spread). The axisymmetric geometry allows the surface shear viscosity (μ^s) to be isolated since it is the only interfacial property that appears in the azimuthal component of the tangential stress balance. The determination of surface shear viscosity from their method is based on the solution for Stokes flow in the channel. In this inertialess limit, the secondary overturning meridional flow is decoupled from the primary azimuthal flow. The deep-channel surface viscometer is considered among the most sensitive methods for the measurement of μ^s, with sensitivity down to 10^{-4} sP on water. Although there is no fundamental upper bound for the measurements of μ^s, the slow rotation of the floor, necessary for the Stokes flow approximation, makes measurements of large values of μ^s impractical for a bulk liquid with relatively small viscosity, such as water. For example, measurement of $\mu^s = 10^{-1}$ sP on water requires approximately 2 h for the tracer particle to travel once around the channel, based on the dimensions of the original channel (radius ≈ 6 cm) operated at 1 rev. $\mathrm{min^{-1}}$ by Mannheimer & Schechter (1970). The long times required for measurements of large μ^s bring about other practical considerations, such as ageing of the monolayer and contamination issues. Another shortcoming in the use of the inertialess (analytical) theory is satisfying the 'deep-channel' restriction, $d/(r_o - r_i) \gtrsim 1$. Decreased depth would offer the advantage of increased surface flow for a given Reynolds number, $Re = \Omega r_o^2/\nu$ (ν is the kinematic viscosity), which would decrease the measurement time and improve the signal-to-noise ratio in the measurement of the tracer particle velocity. However, the secondary flow which is ignored in the inertialess theory then becomes more important. Other discrepancies that can result from the theory of Mannheimer & Schechter (1970), including the effects of

curvature and increased inertia, are discussed by Pintar, Israel & Wasan (1971) and Slattery (1990).

Lopez & Hirsa (1998, 2000) have performed Navier–Stokes simulations as well as measurements (Hirsa, Lopez & Miraghaie 2001) of flow in the deep-channel geometry, with insoluble monolayers, at relatively large Reynolds numbers. Aside from the viscosity in the bulk and μ^s, the flow depends on the equation-of-state (relating the thermodynamic surface tension, $\sigma = \sigma(c)$, to the monolayer concentration), interfacial diffusivity, and the dilatational viscosity. Although, the dependence on κ^s is negligible compared to the elasticity term (surface tension gradient), owing to the small capillary numbers considered ($Ca = \mu\Omega r_o/\sigma_0$, σ_0 is the surface tension of clean water). However, when the initial concentration of the monolayer is large enough for the given *Re*, the flow is radially stagnant and the concentration of the monolayer is essentially uniform on the interface. Under these conditions, the interfacial flow is only in the azimuthal direction and the only interfacial property it depends on is μ^s. Here we exploit this phenomena to extend the dynamic range of the deep-channel viscometer for the measurement of μ^s by operating the channel over a wide range of Ω. The increased utility comes at the price of requiring a (computational) solution of the Navier–Stokes equations, rather than an (analytic) solution to the Stokes problem, owing to the increased inertia in the system. However, today, such computations are routine and can fully account for the dimensions of the apparatus and the operating conditions.

The formulation of the interfacial stress balance is detailed in § 2. To ensure the applicability of the theoretical model, the flow must be axisymmetric, the interface flat, and the radial velocity at the interface zero. In § 3, the experimental set-up is described, and it is shown that over the range of *Re* considered ($Re \in [250, 8000]$) the flow remains steady. The system has only $SO(2)$ symmetry (invariance to arbitrary rotations about the axis), and if this symmetry is broken, a (time-periodic) rotating wave state results (Knobloch 1996; Iooss & Adelmeyer 1998). Hence, a steady flow implies an axisymmetric flow. In § 3, it is also shown that surface deformations and radial surface velocity are measured to be vanishingly small. In § 4, computed solutions of the Navier–Stokes equations at steady state are presented, and the effects of variations in *Re* and μ^s are explored. Section 5 presents measured azimuthal velocity profiles at interfaces with vitamin K_1 and stearic acid monolayers for a range of monolayer concentrations and *Re*, and by comparing these to computed profiles at the same nominal *Re*, the corresponding values of μ^s are determined. For stearic acid, these values of μ^s are compared with data from the literature.

2. Theoretical considerations

The fluid is contained in an annular region of inner radius r_i and outer radius r_o, filled to a depth d. The two cylinder sidewalls are stationary, and the bottom endwall rotates at a constant rate Ω. The top surface of the fluid is exposed to air, and has a surfactant film (insoluble monolayer) on the interface. Initially, everything is at rest, and the monolayer is uniformly distributed with concentration $c_0\,\mathrm{mg\,m^{-2}}$. At time $t = 0$, the bottom endwall is impulsively started.

The governing equations are the axisymmetric Navier–Stokes equations, together with the continuity equation and appropriate boundary and initial conditions. Using a cylindrical polar coordinate system (r, θ, z), the Stokes streamfunction, ψ, the axial angular momentum, $\alpha = rv$, and the azimuthal component of vorticity, η, the

non-dimensional velocity vector is

$$\boldsymbol{U} = (u, v, w) = \left(-\frac{1}{r}\frac{\partial \psi}{\partial z}, \frac{\alpha}{r}, \frac{1}{r}\frac{\partial \psi}{\partial r} \right),$$

and the corresponding vorticity vector is

$$\nabla \times \boldsymbol{U} = \left(-\frac{1}{r}\frac{\partial \alpha}{\partial z}, \eta, \frac{1}{r}\frac{\partial \alpha}{\partial r} \right).$$

The use of ψ and α is convenient in axisymmetric swirling flows; contours of ψ in an (r, z)-plane depict the streamlines of the flow, and contours of α in that plane depict the vortex lines.

We use r_o as the length scale and $1/\Omega$ as the time scale, and define a Reynolds number $Re(= \Omega r_o^2/\nu)$ to non-dimensionalize the axisymmetric Navier–Stokes equations:

$$\frac{\mathrm{D}\alpha}{\mathrm{D}t} = \frac{1}{Re}\nabla_*^2 \alpha, \tag{2.1}$$

$$\frac{\mathrm{D}\eta}{\mathrm{D}t} + \frac{\eta}{r^2}\frac{\partial \psi}{\partial z} - \frac{1}{r^3}\frac{\partial \alpha^2}{\partial z} = \frac{1}{Re}\left(\nabla^2 \eta - \frac{\eta}{r^2} \right), \tag{2.2}$$

where

$$\nabla_*^2 \psi = -r\eta, \tag{2.3}$$

$$\frac{\mathrm{D}}{\mathrm{D}t} = \frac{\partial}{\partial t} - \frac{1}{r}\frac{\partial \psi}{\partial z}\frac{\partial}{\partial r} + \frac{1}{r}\frac{\partial \psi}{\partial r}\frac{\partial}{\partial z},$$

$$\nabla^2 = \frac{\partial^2}{\partial z^2} + \frac{\partial^2}{\partial r^2} + \frac{1}{r}\frac{\partial}{\partial r},$$

and

$$\nabla_*^2 = \frac{\partial^2}{\partial z^2} + \frac{\partial^2}{\partial r^2} - \frac{1}{r}\frac{\partial}{\partial r}.$$

The boundary conditions on the solid boundaries are no-slip, i.e. the normal and tangential derivatives of ψ vanish; $\alpha = 0$ on the stationary cylinder walls and $\alpha = r^2$ on the rotating floor. The azimuthal vorticity η on the solid boundaries is determined by evaluating (2.3) on the boundaries once ψ is known. On the air/water interface, being a material surface, ψ is continuous with its value on the sidewalls, which we set to zero without loss of generality. We shall assume that the interface is flat, and hence the contact angle at the air/water/solid contact line is 90° (in the physical deep-channel viscometer, we fix the location of the contact line with a groove machined above the interface on the cylinder walls; also, the Froude number, $Fr = \Omega^2 r_o^2/gd$ for the range of Re considered is only of order 10^{-5}–10^{-2}). This leaves the conditions for α and η on the interface to be specified.

In our previous studies of this system (Lopez & Hirsa 2000; Hirsa *et al.* 2001) we treated the interface following Scriven (1960), except that we allowed the surface viscosities to vary with the surfactant concentration. For a flat interface, only the tangential stress balance plays a dynamic role. The tangential stress balance in the azimuthal direction is

$$\frac{\partial v}{\partial z} = \hat{\mu}^s \left(\frac{\partial^2 v}{\partial r^2} + \frac{1}{r}\frac{\partial v}{\partial r} - \frac{v}{r^2} \right) + \frac{\partial \hat{\mu}^s}{\partial r}\left(\frac{\partial v}{\partial r} - \frac{v}{r} \right), \tag{2.4}$$

and in the radial direction

$$\eta = \frac{1}{Ca}\frac{\partial \sigma}{\partial r} + (\hat{\mu}^s + \hat{\kappa}^s)\left(\frac{1}{r^2}\frac{\partial^2 \psi}{\partial r \partial z} - \frac{1}{r}\frac{\partial^3 \psi}{\partial r^2 \partial z}\right) - \frac{1}{r}\frac{\partial^2 \psi}{\partial r \partial z}\frac{\partial(\hat{\mu}^s + \hat{\kappa}^s)}{\partial r} + \frac{2}{r^2}\frac{\partial \psi}{\partial z}\frac{\partial \hat{\mu}^s}{\partial r}, \quad (2.5)$$

where Ca $(= \mu \Omega r_o/\sigma_0)$ is the capillary number, $\hat{\mu}^s = \mu^s/\mu r_o$ and $\hat{\kappa}^s = \kappa^s/\mu r_o$. We have found that when the surface has an adequate amount of surfactant, the radial component of velocity on the interface is zero, and the interfacial condition in the radial direction reduces to no-slip, regardless of the physicochemical details of the system (Lopez & Hirsa 2000; Hirsa *et al.* 2001). Thus, instead of (2.5), we have

$$\eta = -\frac{1}{r}\frac{\partial^2 \psi}{\partial z^2} = \frac{\partial w}{\partial z}. \quad (2.6)$$

With the interface suitably covered by the monolayer and the radial surface velocity zero, we neglect any surface concentration gradients. This means that there is no need to solve an advection–diffusion equation for monolayer concentration, and the surface shear viscosity at such an interface is also constant since the concentration is uniform. This allows us to reduce (2.4) to

$$\frac{\partial v}{\partial z} = \hat{\mu}^s\left(\frac{\partial^2 v}{\partial r^2} + \frac{1}{r}\frac{\partial v}{\partial r} - \frac{v}{r^2}\right). \quad (2.7)$$

Now the only interfacial parameter in the system is the surface shear viscosity. In the Mannheimer & Schechter (1970) inertialess theory, this is also true, but here the essential difference is that the inertia of the system redistributes the vortex lines and so the v-profile at the interface requires the solution of the Navier–Stokes equations. However, as in the Stokes limit, we need only measure the azimuthal velocity at the interface to determine μ^s.

3. Experimental apparatus and methods

The experiments reported in this paper were conducted in the same facility used by Hirsa *et al.* (2001) and only the relevant details and refinements are provided here. A diagram of the optical channel is presented in figure 1. The channel was filled with doubly distilled water up to the bottom of the grooves machined in the cylinders which fixed the contact line and ensured an initially flat interface. The grooves were coated with a thin non-wetting film of paraffin. For the flowing system, the maximum deformation of the interface relative to an undisturbed surface was found in azimuthal plane measurements to be less than 2.5×10^{-3} cm, or only 0.2% of the depth for the highest Froude number (Hirsa *et al.* 2001). The radii of the inner and outer cylinders were $r_i = 7.62$ and $r_o = 9.82 \pm 0.01$ cm and the depth-to-gap ratio $d/(r_o - r_i) = 0.5$. The present experiments were conducted with water at $22 \pm 1\,^{\circ}$C, and the resultant kinematic viscosity was $\nu = 9.57 \times 10^{-3}\,\mathrm{cm^2\,s^{-1}}$. The angular rotation rates of the floor were 0.02618, 0.1048, 0.2096 and 0.841 rad $\mathrm{s^{-1}}$ for $Re = 263$ (250), 1056 (1000), 2112 (2000) and 8475 (8000), respectively. The 5% difference between the Re based on measured Ω and r_o and ν at the measured temperature and the nominal Re values in parentheses is comparable to the variation in ν due to temperature uncertainties.

The velocity measurements were conducted using a digital particle image velocimetry (DPIV) system described previously (e.g. see Vogel *et al.* 2001). Since depth-averaging was to be minimized, special care was taken in the present experiment to produce a relatively thin light sheet and to ensure its placement at the air/water interface. A combination of a positive plano-convex lens ($f = 100$ cm) and

	$Re = 250$ (%)	$Re = 1000$ (%)	$Re = 2000$ (%)	$Re = 8000$ (%)
Stearic acid	2.7	2.7	2.5	2.9
Vitamin K_1	2.2			2.8

TABLE 1. The root-mean-square divided by the mean of the interfacial velocity at the midpoint of the annular region over at least a 60 s period, for monolayer covered interfaces at Re as indicated.

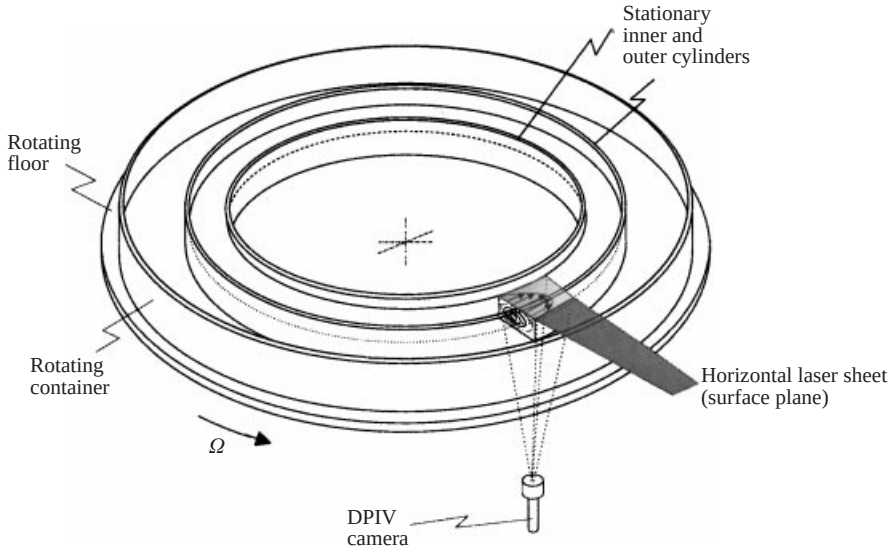

FIGURE 1. The optical annular channel.

a negative plano-cylindrical lens ($f = -6$ cm) was used to produce a light sheet less than 0.04 cm thick. A pair of micro-manipulators were used to mount two razor blades horizontally to form an open slot, whose gap and position were adjusted to a resolution of 10^{-3} cm (10 μm). The horizontal laser light sheet was passed through the slot, which ensured accurate positioning of the light sheet at the air/water interface. For the velocity measurements, the water was seeded with 8.1 μm diameter polystyrene particles (Duke Scientific, 7508A) which were cleaned following the procedure detailed in Hirsa *et al.* (2001).

The surfactants used in the study to form insoluble monolayers were vitamin K_1 (Sigma-Aldrich, 28740-7) and stearic acid (26838-0). Vitamin K_1 was spread using 99^+% pure hexane (13938-6) and stearic acid was spread using HPLC-grade benzene (99.9^+%, 27070-9). In each case, a known amount of the surfactant dissolved in its diluting agent was measured via a glass micro-syringe with Teflon-seal plunger and gradually deposited on the air/water interface. At least 15 min were allowed for the solvent to evaporate and escape from three openings (each 2 cm × 1.5 cm) above the annular region prior to each experiment. It should be noted that due to the nearly neutral pH (6.5–7.0) of the doubly distilled water used in the experiments, the stearic acid monolayer may be partially ionized.

The steadiness of the flow over the range of Re considered was determined by measuring the surface azimuthal velocity at the midpoint of the annular region over at least a 60 s period, with the interface covered with monolayers of vitamin K_1 of

$1.4\,\mathrm{mg\,m^{-2}}$ at $Re = 8000$ and $2.5\,\mathrm{mg\,m^{-2}}$ at $Re = 250$, and stearic acid monolayers at $0.8\,\mathrm{mg\,m^{-2}}$ for a range of Re. The root-mean-square (r.m.s.) divided by the mean of these velocity measurements are given in table 1, where it is seen that for the entire range of cases considered in this study, the flow is steady (and hence axisymmetric). The r.m.s. fluctuations of less than 3% are to be expected, given the 1–2% uncertainty in the velocity measurements.

The DPIV measurements in the plane of the interface provide both the azimuthal velocity profile, V^s, and the radial velocity. For all the cases reported here, the surface radial velocity was zero to within the noise level of the DPIV method.

4. Numerical computations

The numerical solution of (2.1) and (2.2) together with the boundary and interface conditions follows the method used in Lopez & Hirsa (2000) and Hirsa *et al.* (2001), but here the interface conditions are considerably simpler. Specifically, the governing equations are discretized in space using second-order centre differences and temporal integration is via an explicit second-order predictor–corrector scheme which allows for a straightforward implementation of the no-slip condition on the solid boundaries and the interfacial stress balances at the air/water interface. In the annulus of aspect ratio $\Lambda = 0.5$, 201 grid points were used in the radial and 101 in the vertical directions; these were sufficient to resolve all boundary layers at the largest Re considered (8000), and at the lowest Re (250) the flow is considerably over-resolved. The time step used was proportional to Re ($\delta t = 1.5625 \times 10^{-5}$ for $Re = 250$ and $\delta t = 5 \times 10^{-4}$ for $Re = 8000$). The time to reach steady state was also proportional to Re (10 for $Re = 250$ and 250 for $Re = 8000$, corresponding to about 5 to 8 min for the range of Ω used in the experiments). Further details of the numerical method are omitted as they are now standard and detailed elsewhere (e.g. Lopez 1990; Lopez & Weidman 1996; Lopez & Hirsa 1998, 2000).

Figures 2 and 3 summarize the effects of the two parameters Re and $\hat{\mu}^s$ (the geometric parameters were kept fixed at the values corresponding to the experiment). The contours in the three panels are of the streamlines (ψ), the azimuthal component of vorticity (η), and the vortex lines (α). The bottom boundary in each is the rotating floor, and the left- and right-hand boundaries are the stationary inner and outer cylinders, respectively. The top boundary is the air/water interface, modelled to have a uniform monolayer with surface shear viscosity $\hat{\mu}^s$, and to be flat with a radial stress due to both surface tension gradients and surface viscosities that brings the radial velocity at the interface to zero (see Lopez & Hirsa 2000; Hirsa *et al.* 2001). A number of salient features are directly evident. The finite inertia of the system ($Re \neq 0$) drives a secondary overturning flow, corresponding to $\nabla_*^2 \psi = -r\eta$, and boundary layers are established on all the no-slip boundaries and on the interface. This secondary flow intensifies with Re and advects the vortex lines with it. Near the bottom rotating floor, the vortex lines are tilted into the (Ekman) boundary layer. Owing to the stationary outer cylinder, the layer is turned into the vertical direction, and fluid with large angular momentum is brought into the interior (in the Stokes limit, $Re \to 0$, some angular momentum is diffused into the interior, but with inertia significantly more angular momentum is advected in). At the higher $Re = 8000$, the turning of the Ekman layer is observed to result in a jet-like flow of high angular momentum fluid up the outer cylinder wall, which is then turned radially inwards by the interface. This results in the fluid on the interface being spun-up at progressively smaller radii as Re is increased, owing to the bulk advection of angular momentum.

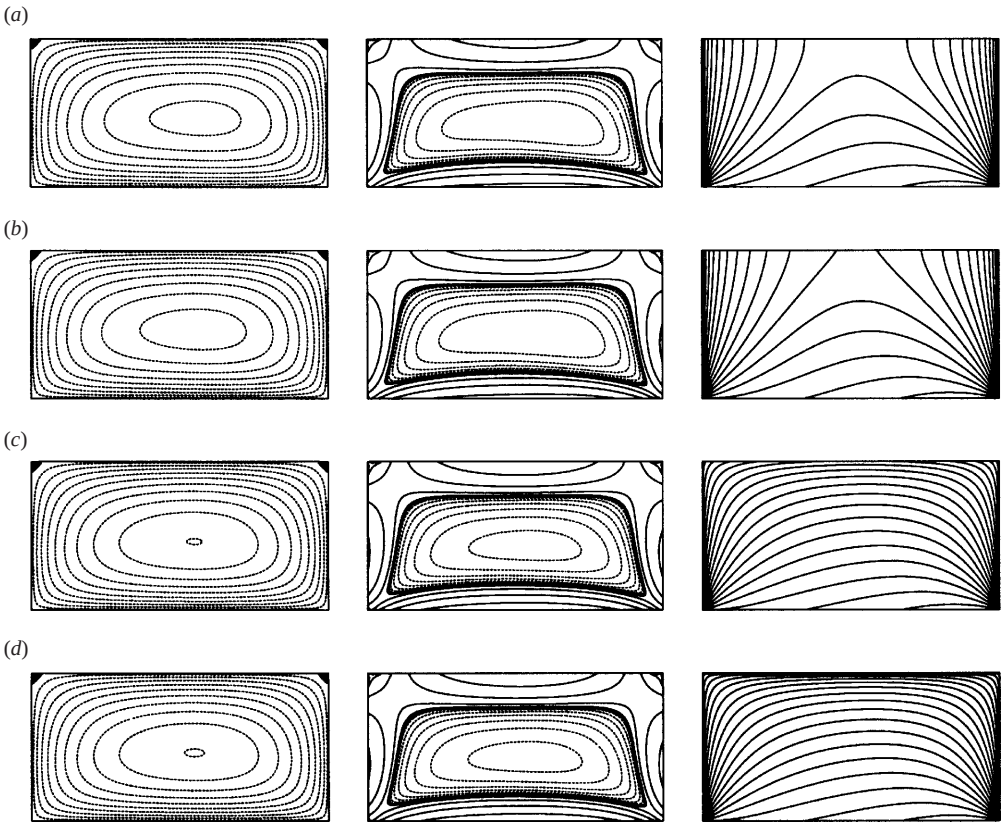

FIGURE 2. Contours of ψ (left-hand side), η (middle), and α (right-hand side), at steady state with $Re = 250$ and (*a*) $\hat{\mu}^s = 0$, (*b*) $\hat{\mu}^s = 10^{-2}$, (*c*) $\hat{\mu}^s = 1$, (*d*) no-slip top.

The other salient feature in the contour plots is the manner in which the vortex lines meet the interface. At a flat, stress-free air/water interface (ignoring viscous effects on the air side), the vortex lines are normal to it, whereas at a no-slip boundary the vortex lines are tangential. Equation (2.7) shows that the slope of the vortex lines at the interface is proportional to the surface shear viscosity and the radial gradients in shear. The vortex lines (contours of α) in the figures at $\hat{\mu}^s = 0$ are normal to the interface, and meet the interface at a sharper angle as $\hat{\mu}^s$ is increased. Also shown are solutions for a no-slip top (with $v = 0$), and note that the limit $\hat{\mu}^s \to \infty$ is the no-slip limit.

The above dependence on inertia ($Re \neq 0$) and $\hat{\mu}^s$ produce a large variation in the azimuthal velocity profile at the interface, and this predicted variation is used to infer μ^s for monolayers at various concentrations by measuring their surface velocity profiles and comparing these to computed profiles. The range of variation is summarized in figure 4 where profiles across the interface ($x = (r - r_i)/(r_o - r_i)$) for $\hat{\mu}^s \in [0, 10]$ and $Re \in [62.5, 16\,000]$ are presented. The lowest Re (62.5) corresponds to the value used by Mannheimer & Schechter (1970) (see also Lopez & Hirsa 1998), and the largest Re (16 000) is the upper bound for steady flow in the present experiments, and the largest $\hat{\mu}^s$ (10) corresponds to $\mu^s \approx 1$ sP. As noted earlier, increased μ^s reduces the surface velocity, and increased inertia spins-up the inner part of the interface.

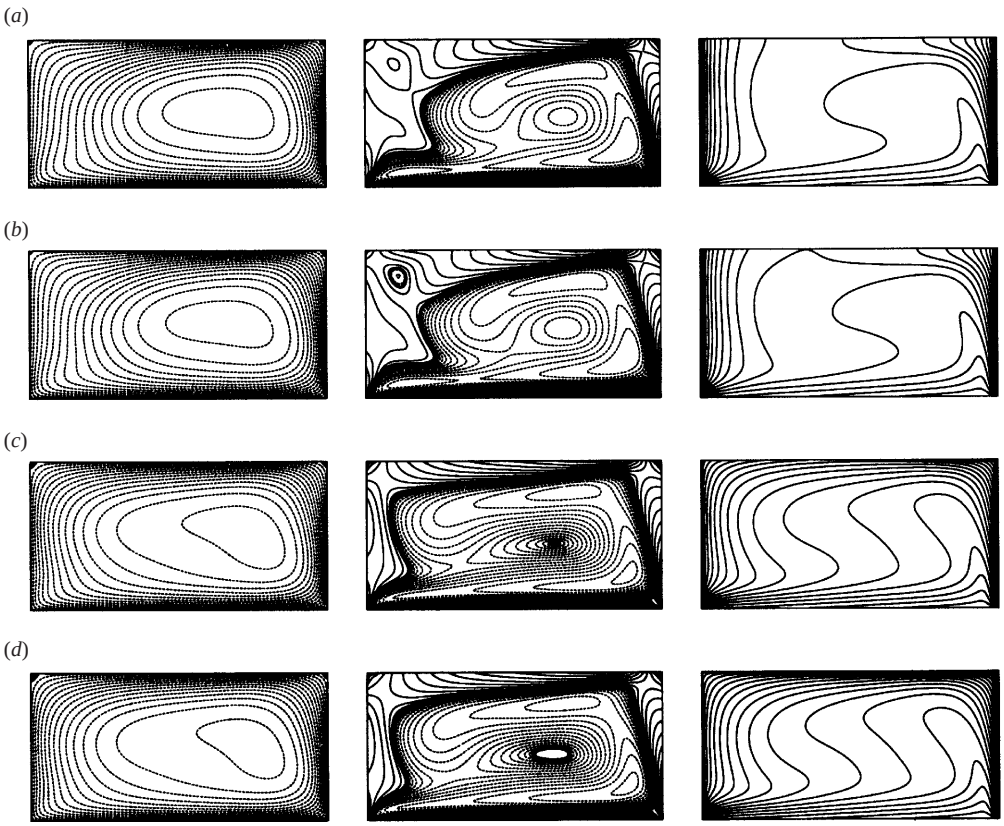

FIGURE 3. Contours of ψ (left-hand side), η (middle), and α (right-hand side), at steady state with $Re = 8000$ and (*a*) $\hat{\mu}^s = 0$, (*b*) $\hat{\mu}^s = 10^{-2}$, (*c*) $\hat{\mu}^s = 1$, (*d*) no-slip top.

5. Determination of surface shear viscosity

Experiments were first conducted using monolayers of vitamin K_1 to establish a baseline for the velocity measurements, since extensive measurements were made by Hirsa *et al.* (2001) at a nominal $Re = 8500$. They showed that for $c_o > 1\,\mathrm{mg\,m^{-2}}$, the radial velocity at the interface diminishes and the concentration distribution is essentially uniform. They also reported that at concentrations less than $1.45\,\mathrm{mg\,m^{-2}}$, vitamin K_1 has negligible surface shear viscosity. Figure 5(*a*) shows the (dimensional) azimuthal component of surface velocity across the annular channel, where X is the dimensional distance from the inner cylinder, for $c_o = 1.4\,\mathrm{mg\,m^{-2}}$ and $Re = 8000$. The agreement between the azimuthal velocity measurements and predictions for $\mu^s = 0$ is reasonably good, considering that the average deviation (|measurement prediction|/|measurement|) between the measurements and predictions (for X up to 19 mm) is 1.9% and that the uncertainty in the measurements is $\pm$1–2%. The deviation between the measurements and prediction increases at large X (i.e. near the outer cylinder); one possible source of error is that some laser light is scattered from the junction between the outer cylinder and the air/water interface, and this scattered light may illuminate seeding particles slightly deeper into the bulk in that region compared to elsewhere along the light sheet. This slight depth-averaging is expected to produce azimuthal velocity with larger magnitude than at the interface.

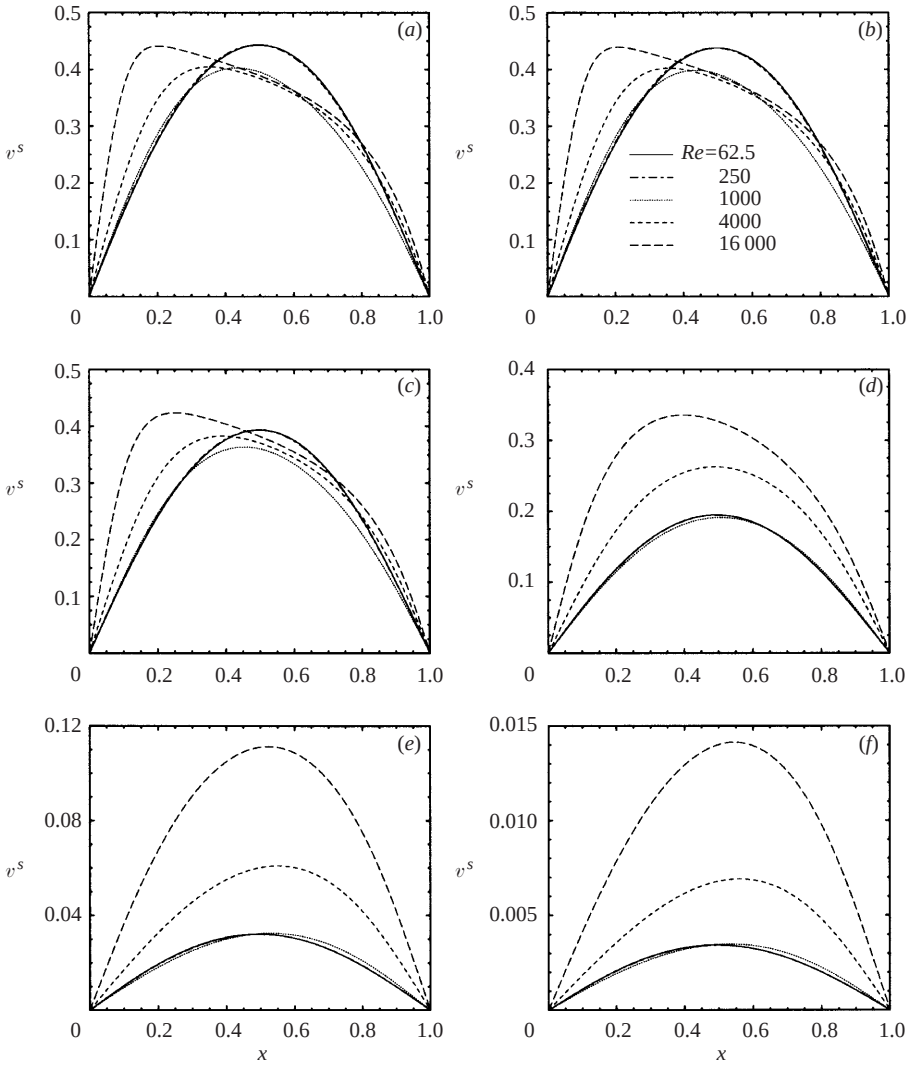

FIGURE 4. Profiles of surface azimuthal velocity, v^s, at various Re and $\hat{\mu}^s$. (*a*) $\hat{\mu}^s = 0$, (*b*) $\hat{\mu}^s = 10^{-3}$, (*c*) $\hat{\mu}^s = 10^{-2}$, (*d*) $\hat{\mu}^s = 10^{-1}$, (*e*) $\hat{\mu}^s = 1$, (*f*) $\hat{\mu}^s = 10$.

Comparison between the measurements and the predictions for different μ^s, namely 0 and $0.01\mu r_0 = 0.94$ milli-surface Poise (msP), indicates that at a concentration of $1.4\,\mathrm{mg\,m^{-2}}$, vitamin K_1 monolayer is essentially inviscid (see figure 5*a*). This confirms the surface shear viscosity measurements by Hirsa *et al.* (2001) which were made using the conventional deep-channel viscometer technique (Stokes flow regime). Figure 5(*b*) shows azimuthal velocity profile for vitamin K_1 at the larger concentration of $2.5\,\mathrm{mg\,m^{-2}}$ tested at a smaller $Re = 250$. For comparison, the computed velocity profiles for $\mu^s = 0$, 0.006 and $0.01\mu r_o$ are presented in the figure. The measurements show the best overall agreement with the $\mu^s = 0.006\mu r_o$ computed profile (which dimensionalized gives $\mu^s = 0.56\,\mathrm{msP}$). Note that this value is close to 0.42 msP which would result from using deep-channel viscometer theory Mannheimer & Schechter 1970), which assumes larger depth and small Re.

Owing to the availability of surface shear viscosity data for stearic acid, a series

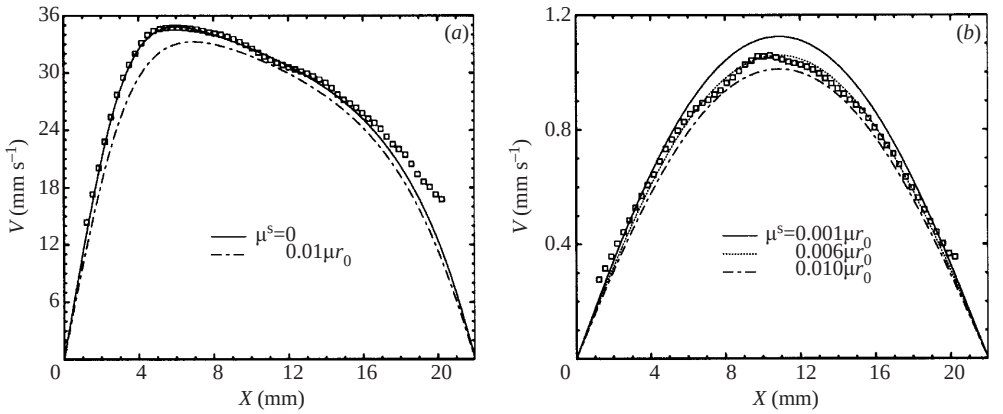

FIGURE 5. Surface velocity profiles (dimensional) for (*a*) $Re = 8000$ with μ^s as indicated (computed, shown as lines) and $c_0 = 1.4\,\mathrm{mg\,m^{-2}}$ of vitamin K_1 (measured, shown as squares) and (*b*) $Re = 250$ with μ^s as indicated (computed, shown as lines) and $c_0 = 2.5\,\mathrm{mg\,m^{-2}}$ of vitamin K_1 (measured, shown as squares).

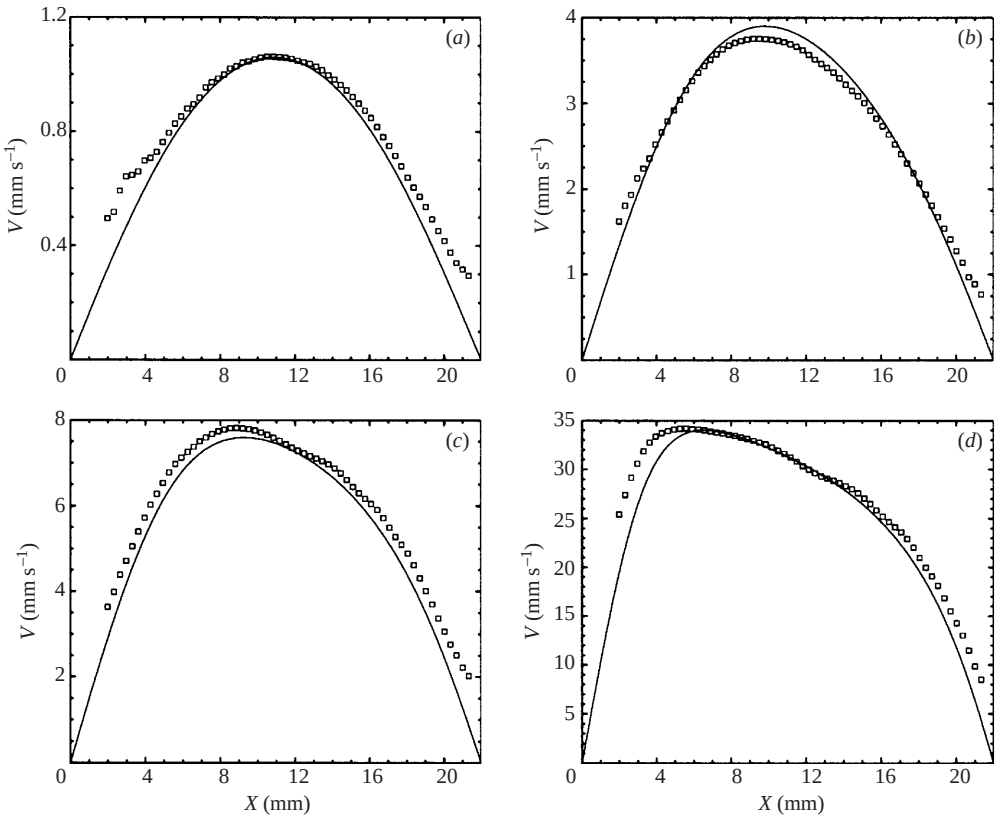

FIGURE 6. Surface velocity profiles (dimensional) for $\mu^s = 0.006\mu r_o$ (computed, shown as solid line) and $c_0 = 0.8\,\mathrm{mg\,m^{-2}}$ of stearic acid (measured, shown as squares), for (*a*) $Re = 250$, (*b*) $Re = 100$, (*c*) $Re = 200$, (*d*) $Re = 8000$.

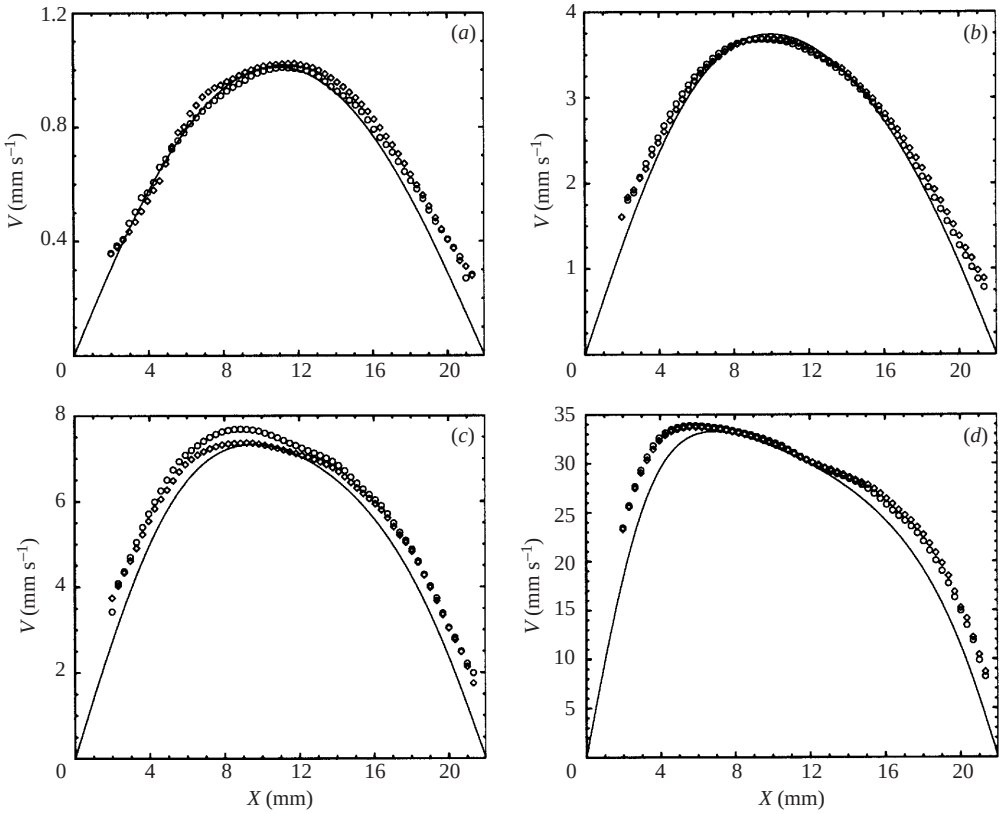

FIGURE 7. Surface velocity profiles (dimensional) for $\mu^s = 0.01$ (computed, shown as solid line) and $c_0 = 1.2\,\mathrm{mg\,m^{-2}}$ (measured, shown as circles) and $c_0 = 1.6\,\mathrm{mg\,m^{-2}}$ (measured, shown as diamonds) of stearic acid, for (*a*) $Re = 250$, (*b*) $Re = 100$, (*c*) $Re = 200$, (*d*) $Re = 8000$.

of measurements were conducted with stearic acid monolayers at various initial concentrations and Reynolds numbers. In figure 6, the azimuthal velocity profiles for a stearic acid monolayer at $c_o = 0.8\,\mathrm{mg\,m^{-2}}$ are shown for Re between 250 and 8000. The generally symmetric profile about the centre of the annular channel for $Re = 250$ (and even at $Re = 1000$), is consistent with the weak secondary flow expected at low Re. The strong secondary flow which occurs at the larger Re and the associated bending of vortex lines (compare the contours of η and α in figure 2*b* and figure 3*b*) can explain the shift in the maximum azimuthal velocity towards the inner cylinder for the larger Re (see figures 6*c* and 6*d*). The single value of surface shear viscosity which best fits the measurements for all Reynolds numbers is $\mu^s = 0.006\mu r_o = 0.56\,\mathrm{msP}$. The agreement between the velocity measurements and the predicted profile is good for $Re = 250$, especially away from the cylinder walls. The uncertainties in the measurements of velocity and initial monolayer concentration may contribute to the small discrepancies seen between the measurements and the predictions. The general agreement for all the Re demonstrates that the stearic acid monolayer on water at this concentration behaves as a Newtonian interface.

The measured velocity profiles for stearic acid monolayers with $c_0 = 1.2$ and $1.6\,\mathrm{mg\,m^{-2}}$ are quite similar, as illustrated in figure 7. The predictions for $\mu^s = 0.01\mu r_o = 0.94\,\mathrm{msP}$ show the best overall agreement for measurements at all four values of Re. The measurements at $Re = 2000$ (figure 7*c*) show some discrepancies

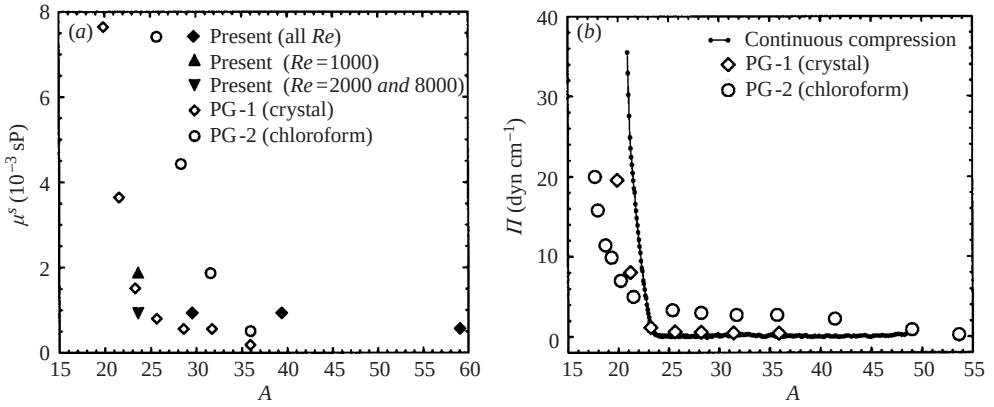

FIGURE 8. (*a*) Variation of surface shear viscosity, μ^s, with surface area coverage, A (Å^2/molecule) for stearic acid monolayers, as measured using the present technique (filled symbols) and as reported in Poskanzer & Goodrich (1975), where the monolayer was spread from its crystal form (open diamonds) and from a chloroform solution (open circles). (*b*) Surface pressure, Π, versus A for stearic acid monolayers measured using continuous compression in a Langmuir trough (solid circles and line), and as reported in Poskanzer & Goodrich (1975), with the monolayers spread as in (*a*).

between the two concentrations, indicating a slightly smaller value of μ^s is applicable for the monolayer with $c_0 = 1.2\,\mathrm{mg\,m^{-2}}$, however, this difference is within the uncertainty in μ^s estimated to be $\pm 0.002\mu r_o$, or about 0.2 msP, consistent with uncertainties in inertialess deep-channel viscometers (Mannheimer & Schechter 1970). Figure 8(*a*) shows the variation of μ^s with A, the area per surfactant molecule (Å^2/molecule), where for stearic acid $A = 47.24\,c^{-1}$, and c is the surfactant concentration in mg m^{-2}. Plotted in the figure are the present measurements of μ^s (filled symbols) together with those from Poskanzer & Goodrich for the two cases where the monolayer was spread from its crystal form (open diamonds) and from a chloroform solution (open circles). The errors in all the measurements are of order ± 0.1 msP. For large A, all measurements show that μ^s diminishes, and for small A, all show that μ^s increases dramatically. The present method at $A = 23.6$ Å^2/molecule ($c_0 = 2.0\,\mathrm{mg\,m^{-2}}$), did not obtain a unique value of μ^s for all Re. For $Re = 250$, the interface was immobile and no value of μ^s could be determined. For $Re = 1000$, $\mu^s = 1.88$ msP was obtained, while for $Re = 2000$ and 8000, $\mu^s = 0.94$ msP, which is substantially smaller. This indicates that at this higher concentration, the stearic acid monolayer is dislaying some non-Newtonian characteristics. This occurs at concentration values where the surface pressure, Π, increases dramatically (figure 8*b*), indicative of a second-order phase transition to a liquid solid as A decreases. A study of another insoluble monolayer, hemicyanine, showed similar non-Newtonian shear thinning behaviour (Lopez, Miraghaie & Hirsa 2002). Considering measurement uncertainties, including that of c_0 which for the present study is $\pm 6\%$, and the uncertainty in the state (phase) of the monolayer, which can depend on, amongst other factors, how it was spread, our measurements are consistent with those reported by Poskanzer & Goodrich (1975).

6. Discussion and conclusion

We have shown here that the axisymmetric deep-channel flow geometry used in the inertialess limit by Mannheimer & Schechter (1970) can be used to extend the upper range of μ^s measurements by the use of relatively large Re. One of the consequences of large μ^s is that for a given rotation rate of the floor of the viscometer, the interfacial

velocity is diminished to a point where it may no longer be measurable. The benefits of driving the viscometer at faster rates are two-fold; for a given (large) μ^s, the measured surface velocity is larger and hence obtained with an improved signal-to-noise ratio, and the measurement times are reduced thus diminishing problems with surface ageing and contamination. These added benefits come at the cost of having to solve (computationally) the Navier–Stokes equations, rather than using analytic surface velocity profiles obtained in the Stokes limit. However, these computations are now straightforward and accurate, and once a set of velocity profiles for a given geometry and Re over a range of μ^s are obtained, the velocity profile from subsequent measurements at that Re can be used to determine the surface shear viscosity.

The present results show that although the flow remains steady and hence axisymmetric (a requirement for the present model) for Re up to about 16 000, the benefits of added inertia diminish since the interfacial velocity becomes insensitive to small changes in μ^s as Re is increased beyond about 2000.

Increasing Re much beyond 2000 can make it likely that the secondary flow is strong enough to produce gradients in the concentration of the monolayer (and perhaps even lead to partial cleaning of the interface), violating the model premise that the radial velocity at the interface is zero and μ^s constant across the interface. The Reynolds number in this study was increased to relatively large values, but we were careful not to apply the technique to very low monolayer concentrations, for which the radial velocity at the interface may be non-zero.

Based on the results, we can conclude that increasing Re by one order of magnitude beyond the $Re = 250$ limit for the inertialess theory, results in one order of magnitude improvement in the signal-to-noise ratio of the azimuthal velocity measurements, required for the determination of larger values of μ^s.

This work was supported by NSF Grants CTS-0116947 and CTS-0116995. We thank Professor Tim Wei for the use of his CCD camera, rescuing this work while ours was being repaired.

REFERENCES

Aris, R. 1962 *Vectors, Tensors, and the Basic Equations of Fluid Mechanics*. Prentice-Hall.

Barentin, C., Ybert, C., Di Meglio, J.-M. & Joanny, J.-F. 1999 Surface shear viscosity of Gibbs and Langmuir monolayers. *J. Fluid Mech.* **397**, 331–349.

Boussinesq, J. 1913 Existence of a superficial viscosity in the thin transition layer separating one liquid from another contiguous fluid. *C. R. Hehbd. Seanc. Acad. Sci.* **156**, 983–989.

Edwards, D. A., Brenner, H. & Wasan, D. T. 1991 *Interfacial Transport Processes and Rheology*. Butterworth–Heinemann.

Gaines, G. L. 1966 *Insoluble Monolayers at Liquid–Gas Interfaces*. Interscience.

Grotberg, J. B. 1994 Pulmonary flow and transport phenomena. *Annu. Rev. Fluid Mech.* **26**, 529–571.

Harkins, W. & Kirkwood, J. 1938 The viscosity of monolayers: theory of the surface slit viscosimeter. *J. Chem. Phys.* **6**, 53.

Hirsa, A. H., Lopez, J. M. & Miraghaie, R. 2001 Measurement and computation of hydrodynamic coupling at an air/water interface in the presence of an insoluble monolayer. *J. Fluid Mech.* **443**, 271–292.

Iooss, G. & Adelmeyer, M. 1998 *Topics in Bifurcation Theory and Applications*, 2nd edn. World Scientific.

Knobloch, E. 1996 Symmetry and instability in rotating hydrodynamic and magnetohydrodynamic flows. *Phys. Fluids* **8**, 1446–1454.

Lopez, J. M. 1990 Axisymmetric vortex breakdown. Part 1. Confined swirling flow. *J. Fluid Mech.* **221**, 533–552.

Lopez, J. M. & Hirsa, A. 1998 Direct determination of the dependence of the surface shear and dilatational viscosities on the thermodynamic state of the interface: theoretical foundations. *J. Colloid Interface Sci.* **206**, 231–239.

Lopez, J. M. & Hirsa, A. 2000 Surfactant influenced gas/liquid interfaces: nonlinear equation of state and finite surface viscosities. *J. Colloid Interface Sci.* **229**, 575–583.

Lopez, J. M., Miraghaie, R. & Hirsa, A. H. 2002 Non-Newtonian behavior of an insoluble monolayer: effects of inertia. *J. Colloid Interface Sci.* **248**, 103–110.

Lopez, J. M. & Weidman, P. D. 1996 Stability of stationary endwall boundary layers during spindown. *J. Fluid Mech.* **326**, 373–398.

Mannheimer, R. J. & Schechter, R. S. 1970 An improved apparatus and analysis for surface rheological measurements. *J. Colloid Interface Sci.* **32**, 195–211.

Pintar, A. J., Israel, A. B. & Wasan, D. T. 1971 Interfacial shear viscosity phenomena in solutions of macromolecules. *J. Colloid Interface Sci.* **37**, 52–67.

Poskanzer, A. & Goodrich, F. C. 1975 A new surface viscometer of high sensitivity: II. Experiments with stearic acid monolayers. *J. Colloid Interface Sci.* **52**, 213–221.

Sacchetti, M., Yu, H. & Zografi, G. 1993 Hydrodynamic coupling of monolayers with subphase. *J. Chem. Phys.* **99**, 563–566.

Schwartz, D. K., Knobler, C. M. & Bruinsma, R. 1994 Direct observation of Langmuir monolayer flow through a channel. *Phys. Rev. Lett.* **73**, 2841–2844.

Scriven, L. E. 1960 Dynamics of a fluid interface. *Chem. Engng Sci.* **12**, 98–108.

Slattery, J. C. 1990 *Interfacial Transport Phenomena*. Springer.

Stone, H. A. 1995 Fluid motion of monomolecular films in a channel flow geometry. *Phys. Fluids* **7**, 2931–2937.

Stone, H. A. & Ajdari, A. 1998 Hydrodynamics of particles embedded in a flat surfactant layer overlying a subphase of finite depth. *J. Fluid Mech.* **369**, 151–173.

Vogel, M. J., Hirsa, A. H., Kelley, J. S. & Korenowski, G. M. 2001 Simultaneous measurement of free-surface velocity and surfactant concentration via a common laser probe. *Rev. Sci. Inst.* **72**, 1502–1509.